Non-hydrolytic sol-gel route to a family of hybrid mesoporous aluminosilicate ethanol dehydration catalysts

Ales Styskalik,[a,b] Imene Kordoghli,[a] Claude Poleunis,[a] Arnaud Delcorte,[a] Denis Dochain,[a] Zdenek Moravec,[b] Julius Vida,[c] Tomas Homola,[c] Carmela Aprile,[d] Luca Fusaro,[d] François Devred,[a] Damien P. Debecker*[a]

[a]Institute of Condensed Matter and Nanosciences (IMCN), Université catholique de Louvain (UCLouvain), Place Louis Pasteur 1, 1348 Louvain-La-Neuve, Belgium

[b]Department of Chemistry, Masaryk University, Kotlarska 2, CZ-61137 Brno, Czech Republic

[c]Department of Physical Electronics, Masaryk University, Kotlarska 2, CZ-61137 Brno, Czech Republic

[d]Department of Chemistry, Unit of Nanomaterials Chemistry, University of Namur, 5000 Namur, Belgium

*Corresponding author (damien.debecker@uclouvain.be).

ABSTRACT

Hybrid materials are intensely studied for potential applications in heterogeneous catalysis. Organic groups at the catalyst surface can modify not only its hydrophilicity, but also acidity, hydrothermal stability, porosity, etc. In some cases, tuning such properties leads to improved catalytic performance. Often, however, the organic moieties are limited to methyl groups introduced via post-grafting. Here, a series of mesoporous hybrid aluminosilicate materials was prepared in one pot by non-hydrolytic sol-gel (NHSG). Aromatic, aliphatic, pendant, and bridging organic groups were incorporated. The presence of the organic groups in the bulk and at the outermost surface of the materials was verified by solid-state NMR, IR, ToF-SIMS, and XPS. The hybrid aluminosilicates were tested as catalysts in the gas phase ethanol dehydration to ethylene, and most of them outperformed the inorganic catalyst benchmark. While a direct influence of surface hydrophobicity (as probed by water sorption and water contact angle measurements) appeared unlikely, characterization of acidity (IR-pyridine) revealed that the improved performance for hybrid catalysts could be correlated with a modification of the acidic properties. The latter are determined by the quality of the dispersion of Al centers in the form of isolated sites in the hybrid silica matrix, which itself appears to be influenced by the presence of organic groups in the non-aqueous synthesis. All in all, this study establishes a "ranking" for a variety of organic groups in terms of their influence on the catalyst activity.

Keywords: acidity; ethanol dehydration; heterogeneous catalysis; hydrophobicity;

nonhydrolytic sol-gel, organic-inorganic hybrid composites.

Introduction

Silica-based organic-inorganic hybrid materials have recently captured considerable attention, in particular in the fields of heterogeneous catalysis, gas sensing, coating and adsorption [1, 2]. In heterogeneous catalysis, many publications have reported a performance boost following the introduction of organic groups into inorganic catalysts. This strategy is especially successful in organic reactions that involve water, which should be repelled from the catalyst surface [3–10].

Methyl groups represent the most widely reported type of incorporated organic moieties. Application of other groups (e.g. longer aliphatic chains, aromatic rings, fluorinated organic groups) has been reported less often. A broadening of the scope of available materials, however, might bring other positive effects: not only hydrophobicity alteration (that may or may not be observed upon methyl groups introduction) [3, 11–13], including also selective adsorption of reactants induced by specific non-bonding interactions (e.g. π-π stacking) [14], but also porosity changes [15, 16], hydrothermal stability improvement [17], or modulation of catalyst sites strength and accessibility [18, 19]. Functional organic groups can bring additional advantages to the final material [20].

Co-condensation sol-gel methods have emerged as promising and straightforward routes for the synthesis of organic-inorganic materials including hybrid catalysts [21, 22]. In the traditional sol-gel methods, performed in aqueous medium, molecular precursors hydrolyze and condense forming a solid material with the desired composition and properties. However, hydrolytic sol-gel methods face two major issues: (i) dissimilar reactivity of different precursors often leads to mixed metal oxides of low homogeneity, and (ii) the high surface tension of water tends to cause pore shrinkage during gel drying. Switching to non-aqueous

conditions can bring a solution to these limitations [23–25]. In these “non-hydrolytic sol-gel” (NHSG) routes, oxo bridges are formed with alternative oxygen donors (not water). The low surface tension of the solvents used for the synthesis makes the drying easier. This, associated with the fact that the degree of polycondensation of the gel is often relatively high in NHSG chemistry, avoids pore collapse yielding highly porous materials usually featuring high pore volumes and large pore diameters. Even more importantly, different precursors (metal alkoxides, amides, halides, organometallics, silanes, and organosilanes) tend to react with similar kinetics, leading to metallosilicate materials with excellent metal dispersion (homogeneity). Various organic groups (including both terminal and bridging, aliphatic and aromatic) have already been incorporated into oxide materials via NHSG routes, and this was reported to lead to interesting properties – high surface areas [15, 20, 26, 27], tunable pore sizes [15, 20, 28], varying hydrothermal stabilities [28], and even in some cases superior catalytic activity [7, 18, 29, 30], selectivity improvement [6, 31–33], and more stable catalytic sites [34–38]. Therefore, as reviewed very recently [25], the NHSG method presents an ideal route to porous organic-inorganic hybrid materials and in particular hybrid catalysts.

Ethanol dehydration to ethylene is an important catalytic process in the context of biorefineries [39–42], but it is also a good model reaction, where the influence of hydrophobicity/hydrophilicity can be studied. Alumina, silica-alumina, and HZSM-5 are frequently employed as catalysts for ethanol dehydration [43, 44]. These fully inorganic materials however face limitations: strongly acidic HZMS-5 are very active but deactivate rapidly, and Al_2O_3 and silica-alumina are more stable but show only modest activity. Hybrid materials featuring both acidic sites and hydrophobic groups on their surface might be good candidates in the dehydration reaction. However, for this reaction, only a handful of reports

in the primary literature mention the application of hybrid catalysts to enhance activity, selectivity, or stability [8, 45–48].

In the specific case of gas-phase ethanol dehydration to ethylene, we have shown that two important factors influence strongly the behavior of hybrid metallosilicates: (i) the hydrothermal stability of Si–C bonds (which is unsatisfactory if aromatic organic groups are directly bound to Si atoms) [28] and (ii) the number, nature, and strength of acid sites [12, 49]. Studying a series of methylated aluminosilicate materials prepared by NHSG, a direct influence of hydrophobicity on the catalytic performance was not demonstrated [12]. Instead, the improved catalytic performance obtained with these hybrid aluminosilicates was attributed to an indirect effect of the presence of $MeSiO_3$ groups, impacting surface acidity.

Moving further, here we broaden the scope of organic modifiers. A series of hybrid aluminosilicates was prepared by NHSG with different organic groups attached to the inorganic matrices: bridging and terminal, aliphatic and aromatic groups were incorporated. The catalysts' structure, porosity, acidity, and hydrophobicity were followed by a number of analytical methods and correlated with performance in ethanol dehydration. By doing so, "a ranking" of organic groups is established according to their effect on catalytic performance, and these hybrid catalysts are benchmarked to the conventional, purely inorganic catalyst (free of organic groups).

Materials and methods

General. Catalyst syntheses were performed under high vacuum or dry N_2 atmospheres using Schlenk techniques or in a dry box with H_2O and O_2 levels below 1 ppm. CH_2Cl_2 was dried with P_4O_{10}. Diisopropyl ether and benzene-d_6 were dried over Na metal. Solvents were distilled and stored in a glovebox over molecular sieves. Aluminum chloride (ABCR, $AlCl_3$, 99.999 %), silicon tetrachloride (Sigma, $SiCl_4$, 99 %), methyltrichlorosilane (Sigma, CH_3SiCl_3, 99 %),

benzyltrichlorosilane (ABCR, $C_6H_5CH_2SiCl_3$, 97 %), bis(trichlorosilyl)methane (ABCR, $Cl_3SiCH_2SiCl_3$, 97 %), and 1,2-bis(trichlorosilyl)ethane (ABCR, $Cl_3SiCH_2CH_2SiCl_3$, 95 %) were stored in a glovebox and used as received. α, α'-dichloro-p-xylene (TCI 98.0 %), tripropylamine (TCI, 98 %), and trichlorosilane (Sigma, 99 %) were used as received for the synthesis of 1,4-bis(trichlorosilylmethyl)benzene according to literature [50]. Ethanol (AnalaR NORMAPUR, 99.95 %) was used as received. Silica-alumina support (grade 135, SA_{BET} = 600 $m^2\ g^{-1}$, V_P = 0.76 $cm^3\ g^{-1}$, Si:Al ratio ~8, **SACS**) was purchased from Sigma-Aldrich. ZSM-5 zeolite in its ammonium form (SA_{BET} = 400 $m^2\ g^{-1}$, Si:Al ratio ~15) was purchased from Alfa Aesar and calcined at 500 °C in order to transform it to H^+ form (**HZSM-5**).

Xerogel synthesis. The xerogels' synthesis methodology was based on our previous report on hybrid aluminosilicates containing $MeSiO_3$ groups [12]; herein the organosilane precursors were varied. Diisopropyl ether (DIPE), organosilane ($R_{pendant}SiCl_3$ or $Cl_3Si–R_{bridging}–SiCl_3$), and silicon tetrachloride were loaded with 45 cm^3 CH_2Cl_2 in an autoclave, in a glove box. $AlCl_3$ (neat) was added to this reaction mixture with vigorous stirring and stirred at RT until complete dissolution (5–10 min). The organic modification degree corresponded in all cases to 1 $R_{pendant}SiO_3$ group (or 0.5 $O_3SiR_{bridging}SiO_3$) for 15 SiO_4 groups, and the Si/Al ratio was 16. These molar ratios were chosen according to our previous study on methylated aluminosilicates [12] and kept constant for all samples prepared in this study. The autoclave was sealed and kept in an oven at 110 °C for 72 hrs for gelation (Eqn. 1). After cooling down, the autoclave was put back into the glovebox, opened and the gel was transferred into a Schlenk vessel. The gels were dried under vacuum at 60 °C overnight in order to remove the solvent and volatile condensation product (isopropyl chloride). The resulting powders were calcined in a dry air flow at 300 °C (1 °C min^{-1}, 5 hrs), yielding brown xerogels. While the molar ratios ($15SiO_4$:$1RSiO_3$:1Al in case of pendant organic groups and $15SiO_4$:$0.5O_3SiR'SiO_3$:1Al in case of bridging organic groups), temperatures, times, etc. were kept constant throughout the whole series of syntheses, the nature of organic groups bound to the silica network was varied. The catalysts are denoted **p_PhCH₂**, **p_Me**, **b_CH₂**, **b_C₂H₄**, and **b_Xy**; the name explicitly refers to the type of organic functionalization (Chart 1), "p" stands for pendant organic groups; "b" stands for "bridging". The incorporated organic moiety is identified by the second part of the name (e.g. benzyl groups "$PhCH_2$", etc.). In order to change the nature of organic groups bound to silica, different organosilane precursors were used: benzyltrichlorosilane,

methyltrichlorosilane, bis(trichlorosilyl)methane, bis(trichlorosilyl)ethane, and 1,4-bis(trichlorosilylmethyl)benzene, respectively. Sample **p_Me** has already been presented in our previous paper, where it was labeled "15Si-1MeSi-1Al") [12]. A purely inorganic benchmark catalyst with the same Si:Al nominal ratio was prepared in the same way using only $SiCl_4$ as a silicon precursor (**16Si-1Al**). Precise reactant masses used in the syntheses can be found in Table 1.

$$AlCl_3 + 15\ SiCl_4 + RSiCl_3 + 33\ {}^{i}PrO{}^{i}Pr \rightarrow \tfrac{1}{2}Al_2O_3{\cdot}15SiO_2{\cdot}1RSiO_{1.5} + 66\ {}^{i}PrCl \quad (1)$$

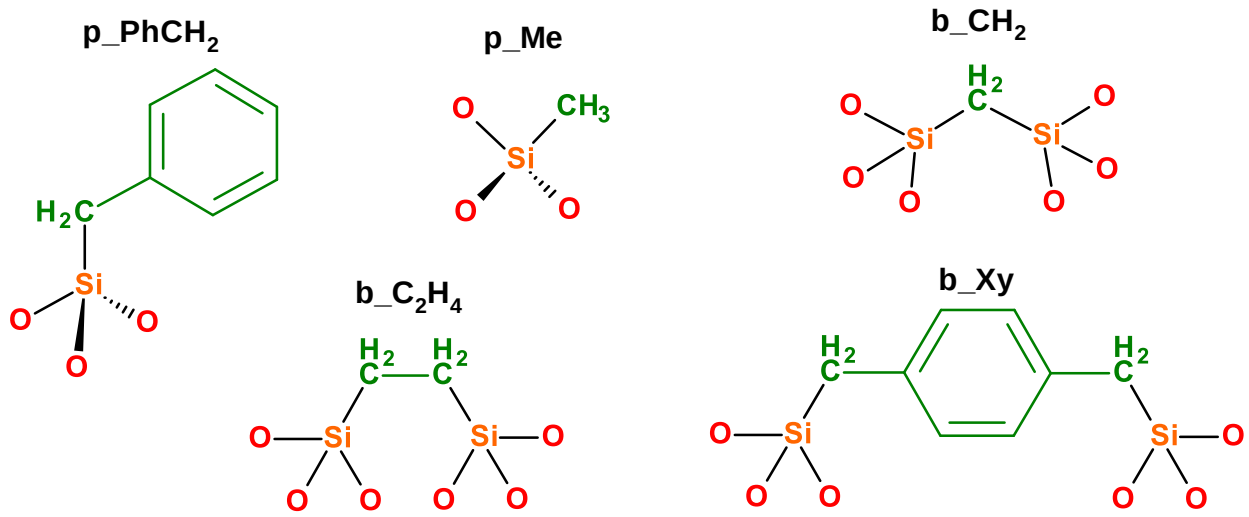

Chart 1: Various organic groups attached to the aluminosilicate matrices and their labeling; p_ stands for pendant organic group, b_ stands for bridging organic group.

Table 1: Synthesis (amount of precursors introduced in the preparation) and the surface composition of hybrid aluminosilicate catalysts (XPS).

Sample	n_{Si} [mmol]	n_{RSi} [mmol]	n_{Al} [mmol]	n_{DIPE} [mmol]	Si/Al ratio Theor[a]/XPS [-]
p_Me[12]	26.87	1.779	1.822	59.89	15.7/24.2
p_$PhCH_2$	26.82	1.809	1.771	59.27	16.2/20.2
b_CH_2	26.66	0.895	1.791	59.14	15.9/24.7
b_C_2H_4	26.84	0.939	1.837	60.08	15.6/28.0
b_Xy	26.88	0.894	1.788	59.02	16.0/25.5

16Si-1Al[12]	28.63	-	1.762	60.09	16.2/30.0

Characterization. Transmission IR spectra (4000–400 cm^{-1}) were recorded on a Bruker Equinox 55 spectrometer and a Bruker Tensor 27 spectrometer from KBr pellets. The same spectrometer was used – in combination with pyridine adsorption – to quantify acid sites [51]. Wafers based on ca. 30 mg of sample were pressed and evacuated overnight at 350 °C at ≈10^{-4} Torr. Then pyridine was adsorbed at its autogenous pressure at room temperature for 30 min. Physisorbed pyridine was removed by evacuation at 150 °C at ≈10^{-4} Torr for 2 hrs and IR spectra were collected. Molar extinction coefficients according to Emeis were used to quantify Lewis acid sites (absorption band at 1455 cm^{-1}) and Brønsted acid sites (absorption band at 1545 cm^{-1}) [51]. The acid sites strength was estimated by further evacuation/IR measurement steps at 250 and 350 °C. Thermal analysis (TG/DSC) was measured on a Netzsch STA 449C Jupiter apparatus from 25–1000 ºC under flowing air (100 $cm^3\,min^{-1}$) with a heating rate of 5 K min^{-1}. Surface areas (SA_{BET}) and pore volumes were determined by nitrogen physisorption at 77.4 K [52, 53] on a Tristar 3000 instrument (Micromeritics, USA). Prior to the measurement, samples were degassed at 150 °C for at least 8 hrs. The specific surface area was determined by the multipoint BET method with at least five data points with relative pressures between 0.05 and 0.30. Water adsorption was performed on a 3Flex instrument (Micromeritics) and Autosorb-iQ3 (Quantachrome) at room temperature (p_0 = 21 Torr). Prior to measurement, the samples were degassed for at least 8 hrs at 150 °C. The ratio of volume of adsorbed liquid H_2O (calculated from H_2O sorption) and volume of adsorbed liquid N_2 (calculated from N_2 sorption) at p/p_0 = 0.3 was denoted "$X_{0.3}$" and taken as a measure of hydrophilicity ("hydrophilicity index") as suggested by Gounder et al. [9], Olson et al. [54] and Thommes et al. [55]. Solution

NMR spectra were recorded on a Bruker Avancelll 300 MHz NMR spectrometer at 299.8 MHz for proton and at 75.4 MHz for carbon with deuterated solvents as the external lock. The proton and carbon NMR spectra were referenced to the residual proton signals or carbon resonances of benzene-d_6 (7.15 and 128.0 ppm, respectively). Solid-state ^{27}Al, ^{29}Si, and ^{13}C solid state magic angle spinning (MAS) NMR spectra were acquired on Bruker Avance-500 NMR spectrometer and Bruker AvanceIIIHD-700 NMR spectrometer with a 4 mm CP-MAS Bruker probe at frequencies 99.4 and 139.2 MHz for Si, 130.3 and 182.6 MHz for Al, and 125.8 and 176.2 MHz for C. MAS rates were 8 kHz for ^{29}Si and ^{13}C (CP)MAS and 10 and 12 kHz for ^{27}Al MAS spectra. Chemical shifts were referenced externally to ^{29}Si δ[3-(trimethylsilyl)-1-propanesulfonic acid sodium salt (DSS)]: 1.53 ppm; ^{13}C δ[adamantane] 38.68 ppm; ^{27}Al δ $[[Al(H_2O)_6]^{3+}$ (aq. solution)]: 0.0 ppm. X-Ray photoelectron spectroscopy (XPS) measurements were carried out on an SSI X probe spectrometer (model SSI 100, Surface Science Laboratories, Mountain View, CA) equipped with a monochromatized Al-Kα radiation (1486 eV). The sample powders, pressed in 4 mm stainless troughs, were placed on an insulating ceramic carousel. The pressure in the analysis chamber was around 10^{-6} Pa. The analyzed area was about 1.4 mm^2 and the pass energy was set at 150 eV. The C1s peak of carbon was fixed to 284.8 eV to set the binding energy scale [56]. Data treatment was performed with the CasaXPS program (Casa Software Ltd, UK) and spectra were decomposed with the least-squares fitting routine with a Gaussian/Lorentzian (85/15) product function and after baseline was subtracted. Time of flight secondary ion mass spectrometry (ToF-SIMS) analyses were conducted with a TOF.SIMS^5 instrument (IONTOF GmbH, Münster, Germany). Sample powders were pressed onto the adhesive part of Post-it® papers. A pulsed Bi_5^+ metal ion source was used to produce a primary beam using an acceleration voltage of 30 kV. An AC target current of 0.07 pA with a bunched pulse width lower than 1 ns was used. Both positive and negative secondary ion

species were analysed. Mass spectra were obtained by scanning the primary ion beam over a 250 x 250 μm^2 area. The total primary ion beam dose for each analyzed area was always kept below $5 \cdot 10^{10}$ ions cm^{-2}, ensuring static conditions. Lateral resolution of ~ 3 µm and mass resolution m/Δm>4000 at 29 m/z were maintained for positive and negative mass spectra acquisition. Charge compensation was conducted using an interlaced electron flood gun (kinetic energy = 20 eV). Data analyses were carried out with SurfaceLab (version 6.5).

Catalytic dehydration of ethanol. The catalytic tests were performed as described elsewhere [12]. Briefly, 0.192 mg of the calcined xerogel catalysts (pressed and sieved in the 0.20–0.40 mm particle size range) were diluted with glass beads (0.5-1 mm) in order to keep a constant volume of catalyst bed. The void space of the reactor was filled with silica beads. The feed consisted of a 40 $cm^3\ min^{-1}$ flow of N_2 into which absolute ethanol (0.212 g h^{-1}) was injected through a NE-300 syringe pump (4.4 mol% of ethanol in N_2). The tests were carried out at atmospheric pressure, WHSV = 1.1 h^{-1}. Temperature was varied stepwise between 205 and 310 °C by steps of 35 °C. Each step consisted of (i) heating ramp (5 °C min^{-1}) and stabilization at the set temperature (21 min) and (ii) steady temperature (56 min). The analysis of the effluent gas was carried out by a VARIAN 3800 Gas Chromatograph equipped with a flame ionization detector (FID) and a Cydex B column (8 injections at each temperature).

Results and discussion

Hybrid aluminosilicate samples were prepared by NHSG with a nominal Si:Al ratio of 16. Various organic groups were introduced (see Chart 1), keeping the degree of functionalization constant: one Si atom out of 16 is bonded to an organic moiety that is either terminal (**p_PhCH$_2$**, **p_Me**) or bridging (**b_CH$_2$**, **b_C$_2$H$_4$**, **b_Xy**). Here, the synthetic procedure is based on the alkyl halide elimination (ether route, Eqn. 1), which is known to produce mixed metal

oxides with high homogeneity of metal mixing and good textural properties (even without requiring the use of a sacrificial templating agent) [23, 24, 57]. Different silicon precursors with covalently bound organic groups were used in the synthesis in order to incorporate various organic groups into the aluminosilicate matrices: benzyltrichlorosilane, methyltrichlorosilane, bis(trichlorosilyl)methane, 1,2-bis(trichlorosilyl)ethane, and 1,4-bis(trichlorosilylmethyl)benzene.[7, 58] The direct Si–$C_{aromatic}$ bond was avoided due to its low hydrothermal gas-phase stability in aluminosilicates [28].

The calcination temperature (300 °C) was chosen to eliminate/oxidize a major part of uncondensed isopropoxy groups coming from the sol-gel preparation while preserving the modifying organic moieties bonded via direct Si–C bonds as confirmed by TG analyses (Table 1S, Fig. 1S). The first mass loss (up to 300 °C) could be attributed to the evaporation of adsorbed water, the organic groups then oxidized between 350 °C and 700 °C. The theoretical and experimental mass losses for samples containing bulky organic groups (**p_PhCH$_2$** and **b_Xy**) appeared to be in good agreement (10.3 vs. 10.2 % and 8.23 vs. 8.89 %, respectively). However, it should be considered that some residual isopropoxy groups were still present in the samples and burned in this temperature range as well, as shown by the 5.10 % mass loss displayed by the pristine sample **16Si-1Al**. Ideally, no mass loss should be observed for fully inorganic catalyst, meaning that the actual contribution of the organic groups is probably lower (see below with NMR quantification).

The samples with different organic groups were almost identical in their textural properties (Fig. 1, Table 2). Specific surface area ranged from 240 to 270 $m^2\ g^{-1}$, total pore volume from 0.60 to 0.77 $cm^3\ g^{-1}$, and average pore size from 9.6 to 12 nm. The isotherm shapes (indicating a high proportion of interparticle voids in total porosity [59]) were very similar to earlier

reported methylated aluminosilicates prepared by the same procedure. The specific surface area decreased only slightly upon organic groups introduction; on the other hand, the total pore volume decreased more markedly (Table 2, Fig. 1).

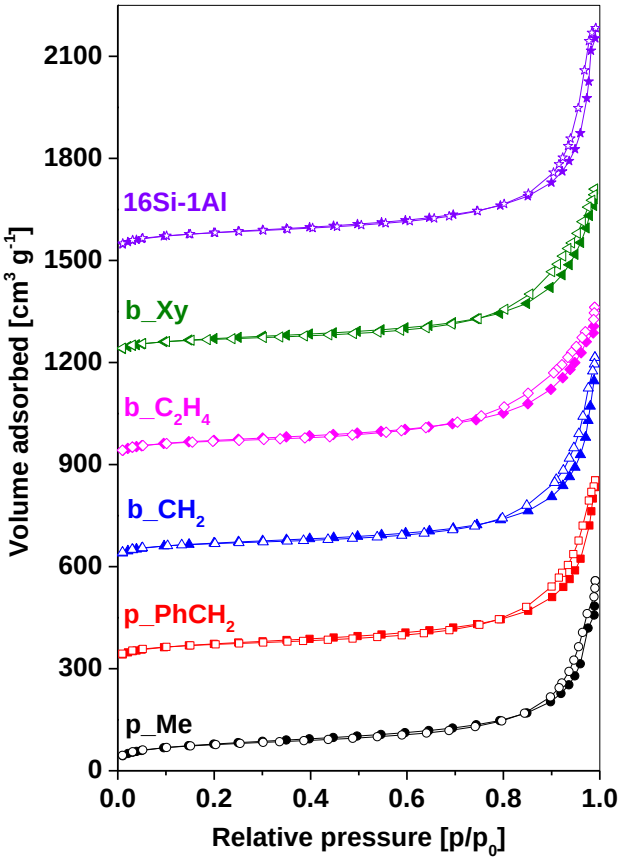

Fig. 1: N_2 physisorption measurements performed on aluminosilicate samples with different organic groups and inorganic benchmark **16Si-1Al**. Empty symbols are used for the desorption isotherms. An offset of 300 $cm^3\ g^{-1}$ has been applied between the isotherms for the sake clarity.

Table 2: Textural properties of NHSG prepared hybrid aluminosilicate samples containing different organic groups.

Sample	SA_{BET} ($m^2\ g^{-1}$)	V_{total} ($cm^3\ g^{-1}$)	D (nm)
p_Me	270	0.75	11
p_$PhCH_2$	250	0.77	12
b_CH_2	240	0.73	12

b_C_2H_4	250	0.60	9.6
b_Xy	250	0.71	12
16Si-1Al	290	0.95	13

Samples with different organic groups were analyzed by IR and NMR spectroscopy and compared to pristine inorganic catalyst. IR spectra (Fig. 2S) of all samples were very similar with the main absorption bands originating from vibrations of aluminosilicate matrix. Spectra were similar to those reported in our previous studies on NHSG-prepared aluminosilicates (both fully inorganic and hybrid) [12, 49]. The intense absorption band at 1050−1065 cm^{-1} can be assigned to the asymmetric stretching vibration of Si−O−Si bridge. This band appears at a lower wavenumber in comparison to pure silica (1200 cm^{-1}); the shift is explained by the presence of Si−O−Al bridges [60–62]. Additional low intensity absorption bands were observed at 570−580, 798−805, and 925−955 cm^{-1} and can be ascribed to Si−O−Si deformation vibration, symmetric Si−O−Si stretching vibration, and Si−O−H stretching vibration, respectively [63]. Finally, absorption bands of very low intensity (KBr pellets) indicated the presence of organic groups in the hybrid aluminosilicate catalysts: 1281 cm^{-1} and 2979 cm^{-1} in **p_Me** (CH_3Si symmetric deformation vibration and CH_3 asymmetric stretching vibration, respectively), 2860 cm^{-1} in **b_CH_2** and **b_C_2H_4** (CH_2 symmetric stretching vibration), 3068 cm^{-1} and 3031 cm^{-1} in **p_PhCH_2** and **b_Xy** (C−H stretching vibrations in aromatic groups). The absorption bands attributed to organic groups were observed with a higher intensity when measuring self-standing wafers based on pure hybrid aluminosilicate catalysts prior to pyridine adsorption (Fig. 3S).

Solid state NMR spectroscopy allowed highlighting the presence of organic groups and verifying their nature. ^{29}Si CPMAS NMR spectra of all samples displayed a main broad signal at –101 ppm (Q2, Q3, and Q4 sites found respectively at –92 ppm, –101 ppm and –109 ppm) accompanied by a minor signal in the range from –45 to –80 ppm confirming the presence of T species ($CSiO_3$) (Fig. 2). ^{29}Si MAS NMR (direct excitation; Fig. 4S) were acquired on **p_Me** and **b_CH$_2$** to indicate the quantity of remaining organic groups (T vs. Q species). Results (Table 1S) must be considered carefully due to the low $RSiO_3$ content and thus a possibly large error during the spectra processing. Nevertheless, the **p_Me** sample showed 55 % of retained organic groups (3 at% experimental vs. 6.02 at% theoretical). These values were lower in the case of **b_CH$_2$** (35 % retained organic groups in comparison to the theoretical value). The rest was probably burned during the calcination step.

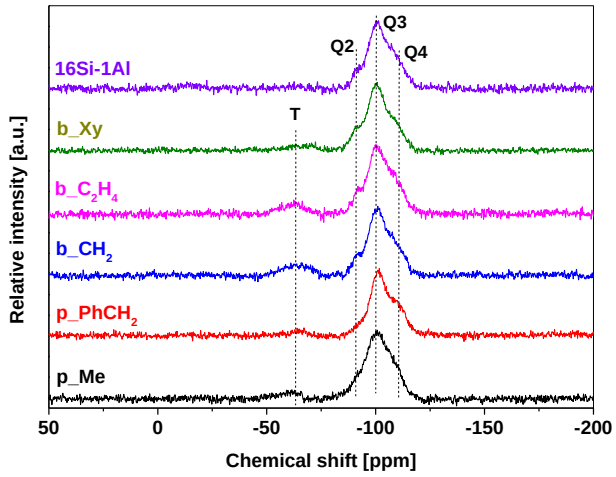

Fig. 2: ^{29}Si CPMAS NMR spectra of NHSG prepared aluminosilicate catalysts with different organic groups.

The nature of the organic groups was identified with the help of ^{13}C CPMAS NMR experiments (Fig. 3). Even if the signal to noise ratio is relatively low (due to the low degree of functionalization), this technique unambiguously allowed to prove that the organic groups bound to the silane precursors used in the synthesis were successfully incorporated within the aluminosilicate matrices and were not subject to any change along the different steps of

preparation (solvothermal synthesis, drying, and calcination at 300 °C). The methyl groups in sample **p_Me** were observed at −5 ppm. The benzyl groups in sample **p_PhCH$_2$** provided two signals at 22 ppm ($C_6H_5\mathit{CH_2}$) and 128 ppm ($\mathit{C_6H_5}CH_2$). Similarly, the xylylene groups in **b_Xy** showed the expected peaks at 19 ppm and 128 ppm [28, 50]. The methylene and ethylene groups in **b_CH$_2$** and **b_C$_2$H$_4$** were observed at –3 and 5 ppm, respectively (Fig. 3) [15, 64, 65].

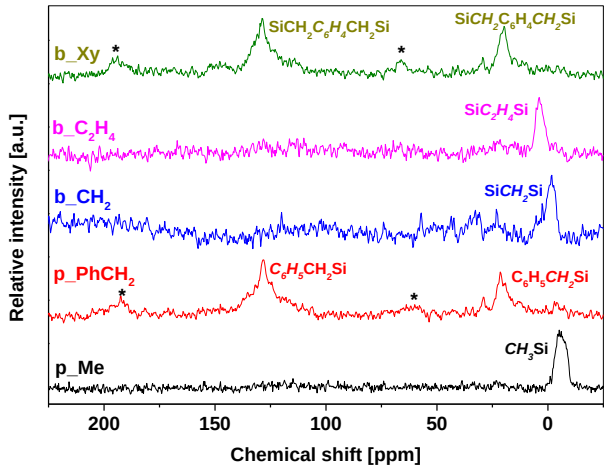

Fig. 3: ^{13}C CPMAS NMR spectra of NHSG prepared aluminosilicate samples with different organic groups. None of the signals detected in hybrid catalysts was present in the pristine **16Si-1Al** catalyst. Asterisks denote spinning sidebands.

According to ^{27}Al MAS NMR spectra (Fig. 4) the NHSG prepared samples, pristine and with different organic groups, were very similar: the framework AlO_4 species were always present as the most intense peak, AlO_5 as a relatively small shoulder, and, finally, the signal intensities of hexacoordinated Al atoms were also comparable.

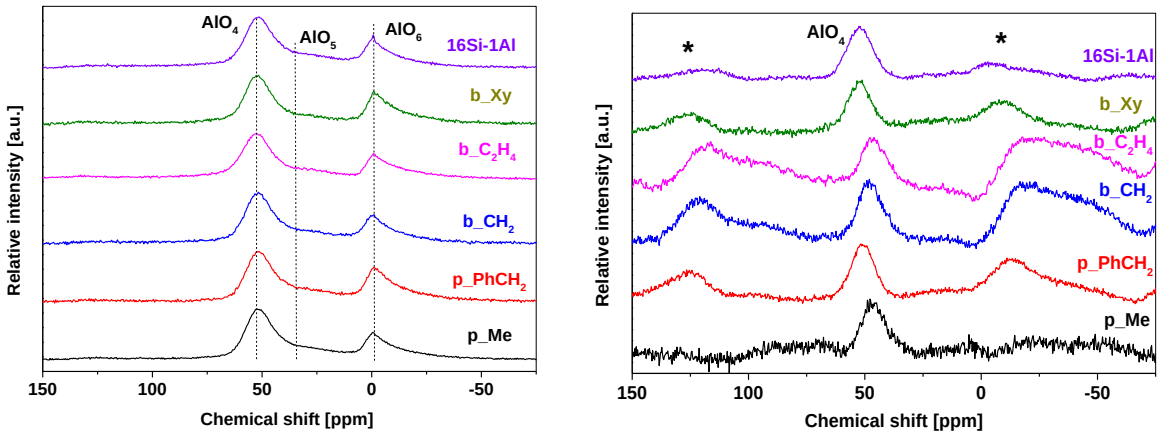

Fig. 4: ^{27}Al MAS NMR spectra of NHSG prepared hybrid aluminosilicate samples with different organic groups. Left: Samples exposed to ambient atmosphere (hydrated); Right: Dehydrated samples with adsorbed pyridine (the low spectra quality and „baseline artifacts“ are present probably due to Al atoms in asymmetrical coordination). Asterisks denote spinning sidebands.

Additional ^{27}Al MAS NMR analyses were performed on dehydrated and consequently pyridine-adsorbed samples. This treatment led to the virtual disappearance of AlO_6 and AlO_5 species both for the hybrid aluminosilicate catalysts and for the inorganic benchmark **16Si-1Al** (Fig. 4, right). This behavior indicated that a formation of extra-framework alumina clusters is excluded in NHSG prepared aluminosilicates (both fully inorganic and hybrid with different organic groups). In fact, octahedrally coordinated Al atoms observed in these samples exposed to the ambient atmosphere (but not in dehydrated catalysts) are isolated Al species able to bind H_2O molecules from air moisture: the coordination of water molecules was fully and rapidly reversible on dehydrated samples (if no pyridine adsorbed), similar to some zeolites [18, 66, 67]. This again pointed towards the fact that NHSG leads to homogeneous Si-Al mixing, with a thorough dispersion of Al in the silica matrix.

While NMR spectroscopy has shown the successful incorporation of organic groups within the bulk of the samples, XPS and ToF-SIMS provide information on the organic groups present at the catalyst surface. Such information is crucial, considering the decisive role played by the

surface in heterogeneous catalysis. In the XPS spectra (Fig. 5), all hybrid samples exhibited a higher C content (Table 3) in comparison to pristine **16Si-1Al** (which only showed the carbon contamination usually encountered in XPS measurement on aluminosilicate materials). The difference was clearly caused by the C–(C,H) component of the carbon peak, which grew in intensity upon the introduction of organic groups. Moreover, an aromatic shake-up component was observed for the samples **p_PhCH$_2$** and **b_Xy**, evidencing the successful incorporation of aromatic moieties. The contribution of the other oxidized carbon types (C–(O), C=O, and COO) typically found in carbon contamination remained fairly constant (1.80–3.78 at%; Fig. 5, Table 3). Thus, the presence of the organic moieties at the surface of the hybrid catalysts is confirmed.

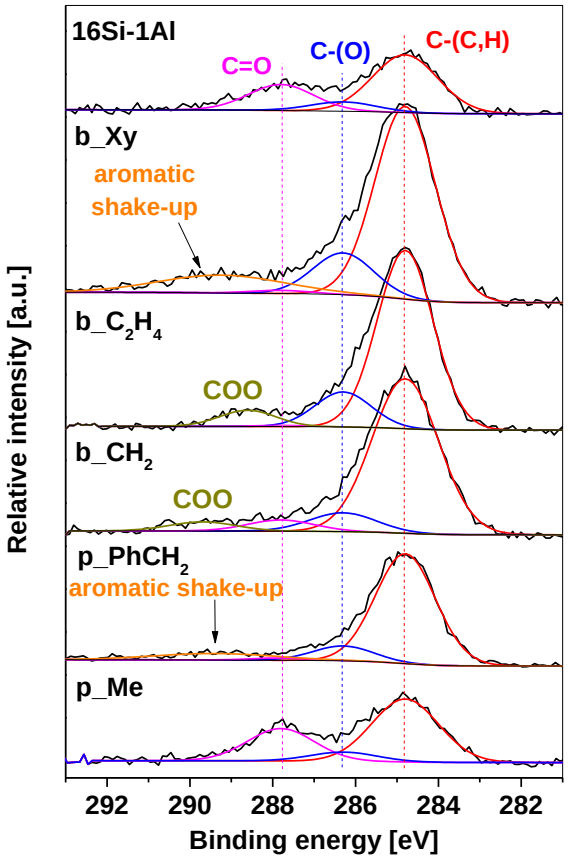

Fig. 5: XPS spectra (C 1s) of NHSG prepared hybrid aluminosilicates with various organic groups. C–(C,H) contribution (set to 284.8 eV) is depicted in red. C–(O) component (binding energy higher by 1.5 eV) is displayed in blue, C=O (binding energy higher by 3 eV) in pink, and COO (binding energy

higher by 4-5 eV) in brown. The aromatic shake-up (a broad component shifted by 4.4-4.6 eV from the C–(C,H) contribution) is shown in orange.

Table 3: Carbon contents in NHSG prepared hybrid aluminosilicate catalysts from XPS data.

Sample	C content total (at%)	C-(C,H) content (at%)	C aromatic shake-up (at%)
p_Me	5.9	3.6	-
p_$PhCH_2$	15.4	12.1	1.5
b_CH_2	13.8	11.0	-
b_C_2H_4	13.7	10.5	-
b_Xy	12.3	8.6	1.7
16Si-1Al[12]	4.7	2.9	-

The introduction of organic groups was further studied by ToF-SIMS, which proves the outermost catalyst surface. Peaks of $C_6H_5^+$ and $C_4H_3^+$ (at m/z 77.037 and 51.026, respectively) indicate the presence of aromatic organic groups (relevant for **p_PhCH₂** and **b_Xy**; Fig. 6a left and Fig. 5S) and peaks of CH_2^+ and $SiCH_2^+$ (at m/z = 14.015 and 41.986) can be used as an indication of the presence of Si–CH_2 moieties (relevant for all hybrid aluminosilicate catalysts; Fig. 6S and 7S). On the one hand, the relative peak areas (normalized per total counts in mass spectra) of $C_6H_5^+$ and $C_4H_3^+$ clearly confirmed the presence of aromatic groups (benzyl and xylylene) in the outermost surface layer of **p_PhCH₂** and **b_Xy** (Fig. 6a, Fig. 5S). On the other hand, the comparison of relative peak areas of CH_2^+ and $SiCH_2^+$ in hybrid samples and **16Si-1Al** does not allow to confirm the presence of organic groups in the outermost surface layer of hybrid samples as the values fluctuate without any clear trend (Fig. 6S and 7S). This is probably due to a high background originating from carbon contamination.

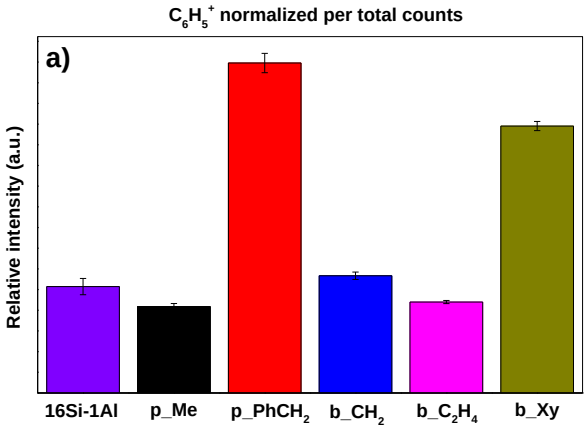
$C_6H_5^+$ normalized per total counts
a)
Relative intensity (a.u.)
16Si-1Al
p_Me
p_PhCH2
b_CH2
b_C2H4
b_Xy

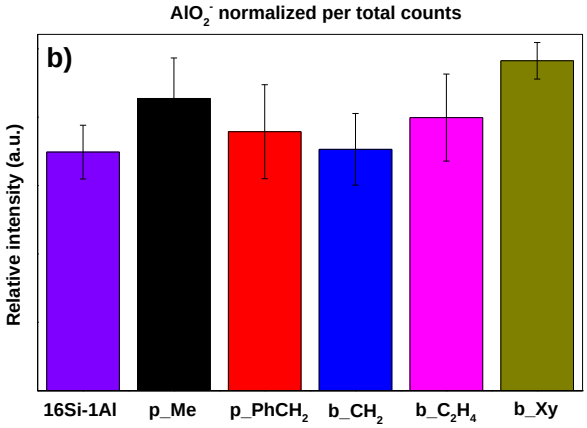
AlO_2^- normalized per total counts
b)
Relative intensity (a.u.)
16Si-1Al
p_Me
p_PhCH2
b_CH2
b_C2H4
b_Xy

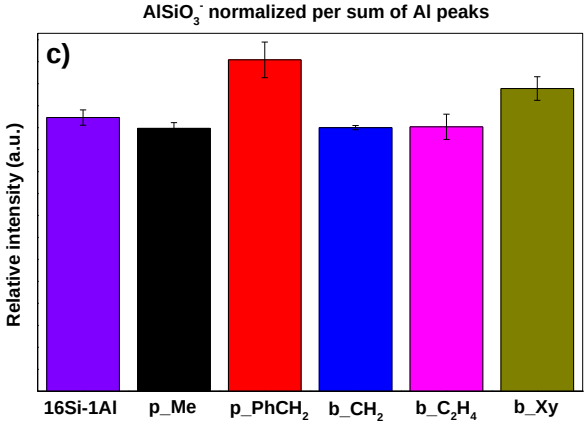
$AlSiO_3^-$ normalized per sum of Al peaks
c)
Relative intensity (a.u.)
16Si-1Al
p_Me
p_PhCH2
b_CH2
b_C2H4
b_Xy

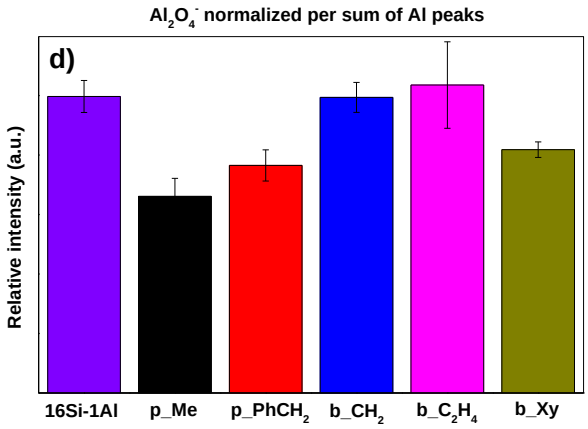

Fig. 6: Comparison of samples with different organic groups in terms of relative peak areas of masses corresponding to a) $C_6H_5^+$ ions, b) AlO_2^- ions, c) $AlSiO_3^-$ ions (mixed Al-Si clusters), and d) $Al_2O_4^-$ ions ("alumina" clusters) in mass spectra obtained by ToF-SIMS. The non-zero values in case of $C_6H_5^+$ peak areas in samples without any aromatic groups probably originate from carbon contamination.

ToF-SIMS was further used to study the homogeneity of Al mixing within silica matrices. Peaks of $(AlSiO_3)^-$, $(AlSi_2O_5)^-$, $(Al_2O_4)^-$, and $(AlO_2)^-$ were followed at m/z = 102.94, 162.92, 117.95, and 58.967, respectively. These signals were well resolved, without any overlap, and undoubtedly assigned. The signals of $(AlSiO_3)^-$ and $(AlSi_2O_5)^-$ are taken as an indication of the presence of Al species incorporated in the silica matrix (which can be associated with homogeneity of the aluminosilicate catalysts). The signal of $(Al_2O_4)^-$ is taken as an indication of the presence of alumina clusters (poorly dispersed Al oxide species). Finally, the signal of $(AlO_2)^-$ is a function of Al concentration in the surface layer and serves as a benchmark. Clearly, all hybrid samples displayed a similar or higher concentration of $(AlO_2)^-$ in comparison to the pristine **16Si-1Al** sample (Fig. 6b). Thus, it can be suggested that hybrid samples possessed at least the same surface Al concentration as **16Si-1Al**. This fact is in agreement with XPS data, where Si/Al ratios for all hybrid samples were lower than for pristine catalyst (Table 1).

Reporting the peak areas of the mixed Al-Si ions vs. the sum of these four peaks containing Al (Fig. 6c, Fig. 8S) it appears that the samples containing aromatic organic groups (**p_PhCH$_2$** and **b_Xy**) display a higher proportion of mixed clusters in comparison to other samples (including the inorganic benchmark **16Si-1Al**). The opposite trend was obtained for $(Al_2O_4)^-$ peak areas: samples with aromatic organic groups displayed a lower amount of alumina clusters per aluminum atoms in the surface layer than other hybrid samples (Fig. 6 d). Thus, the homogeneity of Si-Al mixing appears to be slightly improved in **p_PhCH$_2$** and **b_Xy** samples; the other catalysts seem to display a similar Si-Al dispersion to **16Si-1Al** benchmark sample. Notably, the quality of the Si-Al mixing appears to be at least as good in the hybrid samples as in the inorganic benchmark, showing that the introduction of organic moieties did not deteriorate the homogeneity of the metallosilicate, which is a decisive advantage of NHSG. Overall, the ToF-SIMS analyses of NHSG prepared hybrid aluminosilicate catalysts showed a similar or higher surface Al concentration and similar or higher Si-Al mixing homogeneity in comparison to the pristine **16Si-1Al** sample.

The number of acid sites (determined by IR spectroscopy combined with pyridine adsorption) in hybrid aluminosilicate catalysts ranged between 0.035 and 0.049 mmol g^{-1} (Table 4, Fig. 9S and 10S). The pristine sample **16Si-Al** was the least acidic (0.035 mmol g^{-1}). Moreover, samples containing aromatic organic groups exhibited somewhat higher numbers, while catalysts with aliphatic groups displayed a lower quantity of acid sites. These results are in good agreement with XPS and ToF-SIMS analyses: the hybrid samples showed a higher surface Al concentration (Table 1), aluminosilicate catalysts containing aromatic groups displayed more homogeneous Si-Al dispersion, and, consequently, all hybrid samples possessed higher acid site numbers than pristine catalyst with the maxima observed for **p_PhCH$_2$** and **b_Xy**. Note that this latter trend is even more pronounced if acidity values are normalized by the specific surface area.

Table 4: Results of IR spectroscopy combined with pyridine adsorption performed on hybrid aluminosilicates containing different organic groups.

Sample	Total acid sites (mmol g^{-1})	B/L ratio (-)	Acid sites after desorption at 350 °C (%)	B/L ratio after desorption at 350 °C (-)
p_Me	0.035	0.40	70	0.16
p_$PhCH_2$	0.049	0.37	73	0.20
b_C_2H_4	0.036	0.36	63	0.13
b_Xy	0.045	0.29	58	0.13
16Si-1Al	0.035	0.83	72	0.17
p_$PhCH_2$-500	0.090	0.22	65	0.04
16Si-1Al-500	0.059	0.83	65	0.21

Both Brønsted and Lewis acid sites are present in hybrid aluminosilicates prepared by NHSG. The Brønsted-to-Lewis (B/L) ratio ranges from 0.29 to 0.37, indicating a similar representation among the samples (Table 4). Brønsted acid sites display lower strength than Lewis acid sites; indeed, the B/L ratio decreases in all cases upon evacuation at 350°C. The acid site strength is also similar among the samples with different organic groups: in all samples, a relatively high pyridine fraction (58–73 %) stays adsorbed at the acid sites after evacuation.

While the acid site strength in the fully inorganic **16Si-1Al** catalyst lies within the range of acid site strengths in hybrid aluminosilicates, the B/L ratio is substantially higher in **16Si-1Al** catalyst (0.83) than in all hybrid catalysts (Table 4). This effect has already been observed in the case of methylated aluminosilicates prepared by NHSG [12], and explained with the help of IR spectroscopy: Brønsted acidity in amorphous aluminosilicates is usually explained by the presence of pseudo-bridging Si–OH…Al bridges, where Al atom behaves as a Lewis acid [68–

70]. So, the substitution of Si–OH moieties with Si–R groups provides aluminosilicates with a lower B/L ratio. Accordingly, the intensity decrease of absorption band associated with isolated SiO−H stretching vibration has been observed in this sample series upon organic groups introduction (Fig. 3S).

Water adsorption was investigated on hybrid aluminosilicates to probe their hydrophilic/hydrophobic properties (Fig. 7). The shape of the isotherms indicated no marked change in surface hydrophilicity upon various organic groups introduction: the isotherms always started with a steep increase at the low p/p_0 and copied the shape of N_2 adsorption isotherms in all cases. A measure of hydrophilicity can be derived from water and nitrogen sorption data by calculating the ratio "volume of adsorbed H_2O to volume of adsorbed N_2" at given relative pressure (p/p_0) [9, 54, 55]. This "hydrophilicity index" is here calculated and reported in p/p_0 range from 0 to 0.5 (noted "$X_{p/p0}$"; Fig. 11S). Such ratio is here fully relevant since the texture of the materials is similar in all cases. The hydrophilicity index at $p/p_0 = 0.3$ is reported in Fig. 7 for each catalyst. The value ranges from 32 to 47 % only and is very similar to $X_{0.3}$ of pristine sample **16Si-1Al** (39 %), indicating only minor changes in hydrophilicity upon organic groups introduction, similar to our previous report on methylated aluminosilicates [12].

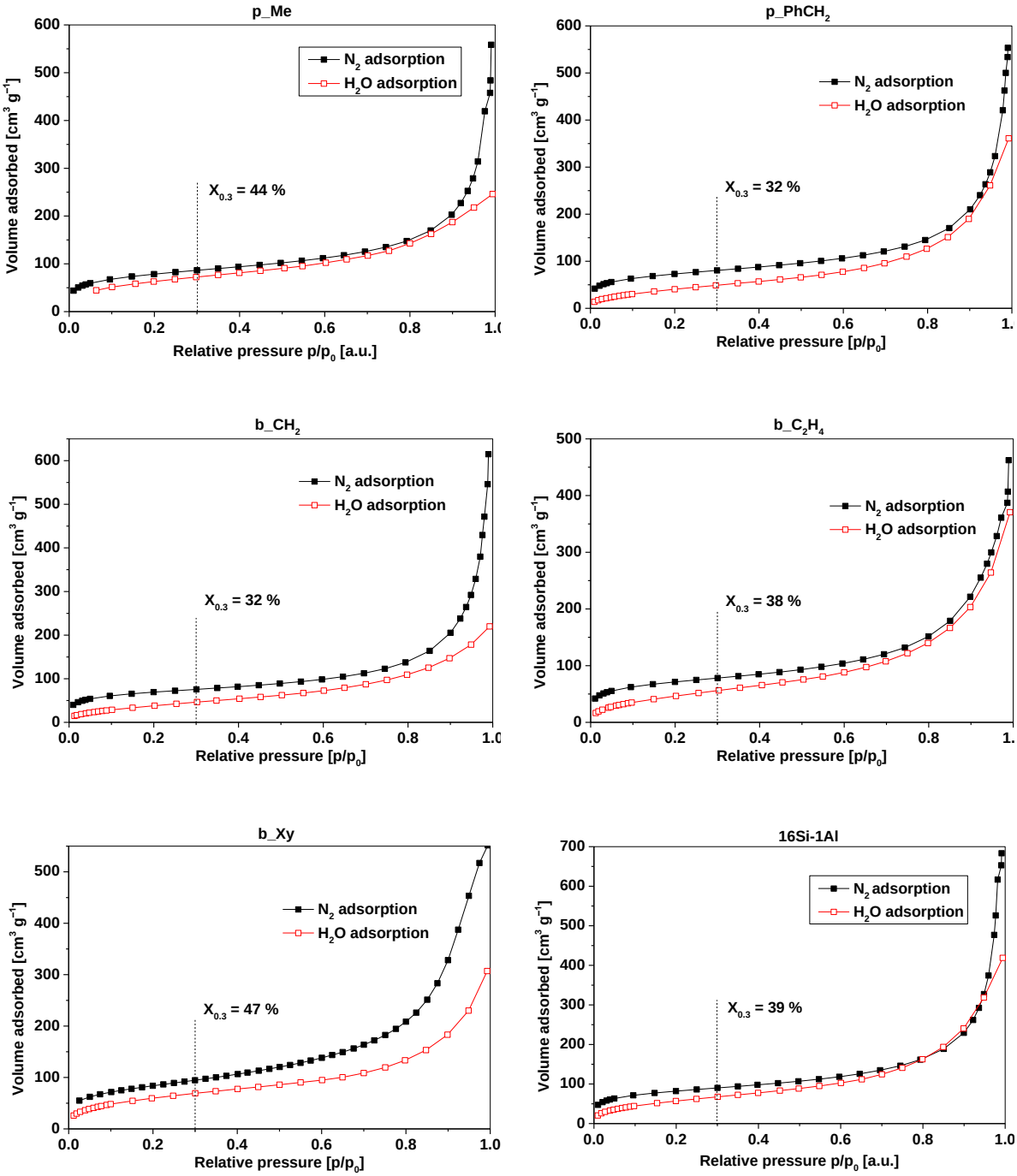

Fig. 7: Comparison of N_2 (solid symbols) and H_2O (open symbols) adsorption isotherms for NHSG prepared aluminosilicates with various organic groups. „Hydrophilicity index" $X_{0.3}$ was calculated as a ratio of volume of adsorbed H_2O and volume of adsorbed N_2 at 0.3 p/p_0 [55]. In this calculation, both adsorbates are being considered as in liquid phase.

The water contact angles were recorded to complement the water sorption experiments (on samples contacted with ambient air and pelletized). Aluminosilicate catalysts with various

organic groups were all found to remain hydrophilic, with water contact angles in the 22-48° range. Samples **p_Me**, **b_C_2H_4**, and **b_Xy** exhibited very similar water contact angles to pure inorganic benchmark catalyst **16Si-1Al** (21.5±1.7 °). Hybrid aluminosilicates **p_$PhCH_2$** and **b_CH_2** exhibited somewhat higher contact angles indicating lower hydrophilicity (35.3±4.7 and 47.6±4.4 °, respectively, Fig. 12S). Interestingly, these two samples displayed slightly lower hydrophilicity according to the "hydrophilicity index" derived from water sorption measurements as well.

The NHSG-prepared aluminosilicate catalysts (both fully inorganic and hybrid) were tested in ethanol dehydration between 205 and 310 °C. Only ethylene and diethyl ether were observed as products (no acetaldehyde, propene, or butenes). Carbon balances fluctuated in the range from 93 to 104 %. Diethylether selectivity was higher at lower temperatures, while ethylene formation was favored at higher temperatures (Table 2S), in accordance with other studies on ethanol dehydration [67, 71, 72]. This general behavior can be explained by reaction enthalpy (exothermic for diethylether formation, but endothermic for ethylene production) [71].

The catalytic performance of hybrid samples in the gas phase ethanol dehydration was compared to inorganic benchmark **16Si-1Al** (Fig. 8). On the one hand, samples containing aromatic organic groups (**p_$PhCH_2$** and **b_Xy**) and **p_Me** showed higher ethylene yields than **16Si-1Al** (Fig. 8). The ethylene yield over **p_Me**, **p_$PhCH_2$,** and **b_Xy** improved mainly due to markedly higher ethylene selectivity (Fig. 13S, right) in comparison to the inorganic benchmark. The ethanol conversion was slightly higher in samples containing aromatic and pendant methyl groups as well (Fig. 13S, left). On the other hand, the catalyst with $SiCH_2CH_2Si$ (**b_C_2H_4**) groups exhibited lower catalytic performance. The sample with methylene bridges (**b_CH_2**) reached a similar ethylene yield to **16Si-1Al** (Fig. 8); it was only slightly worse than

16Si-1Al in terms of ethanol conversion (Fig. 13S, left) but exhibited somewhat better ethylene selectivity (Fig. 13S, right). Any direct effect of the presence of organic groups on the catalytic properties (e.g. enhanced water desorption) seems to be unlikely; the catalytic performance showed correlation neither with hydrophilicity indices $X_{p/p0}$ nor with water contact angles. Overall, the results obtained for hybrid aluminosilicate catalysts mostly follow the acidic properties: hybrid samples with a higher amount of acid sites and a lower B/L ratio perform better (Table 4). The only exception is **b_C_2H_4** which performs worse than expected on the base of its acidic properties. Finally, the selectivity improvement for **p_Me**, **p_$PhCH_2$**, and **b_Xy** might be explained by the marked lowering of the B/L ratio in the case of the hybrid samples: catalysts with more abundant strong Lewis acid sites have been shown to produce ethylene with higher selectivity [12, 49, 67, 72]. The indirect effect of organic groups introduction on catalytic activity in alcohol dehydration was observed by Sow et al. similar to this report: while the activity in 1-butanol dehydration increased for sulfonated ethylene-bridged silica in comparison to SBA-15 silica-based catalyst, the heat of water adsorption remained unchanged [47]. In contrary, van Grieken et al. reported that catalytic activity in production of mixed ethers from 1-hexanol and benzylalcohols over sulfonated hybrid silica materials increased with raising hydrophobicity, as probed by H_2O-TPD measurements [46].

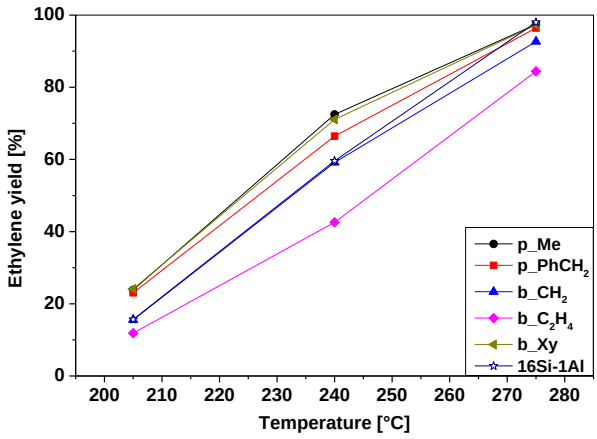

Fig. 8: Ethylene yield in gas phase ethanol dehydration over hybrid aluminosilicate catalysts prepared by NHSG. Black circles denote catalyst p_Me, red squares p_$PhCH_2$, blue triangles (up) b_CH_2, pink diamonds b_C_2H_4, brown triangles (left) b_Xy, and violet stars (empty) denote 16Si-1Al inorganic benchmark.

To confirm that the organic groups' presence (hydrophilicity/hydrophobicity) had a negligible direct effect on catalytic performance, **p_$PhCH_2$** was calcined at 500 °C in order to completely remove organic groups and the resulting catalyst (**p_$PhCH_2$-500**) was tested again in ethanol dehydration. As a reference, **16Si-1Al** was also re-calcined and re-tested (compare samples **p_$PhCH_2$-500** and **16Si-1Al-500**). The calcined **p_$PhCH_2$** again produced ethylene in a higher yield than calcined **16Si-1Al** (Fig. 9). The difference in ethylene yield was caused by varying ethanol conversion: The sample **p_$PhCH_2$-500** remained markedly more active than the calcined **16Si-1Al** (Fig. 14S, left). This agrees with the fact that sample **p_$PhCH_2$** contained more acid sites than **16Si-1Al** both before and after calcination (Table 4). In other words, the organic groups somehow modify the NHSG process – probably owing to a change in the precursors' reactivity – which directly affects the catalyst properties (homogeneity, amount of surface acid sites), and therefore indirectly affects catalytic performance. However, the ethylene selectivity was very similar for both calcined samples (Fig. 14S, right). This is in agreement with our observation that hybrid samples (before calcination) exhibit a higher ethylene selectivity because of lower B/L ratios. This influence was not observed anymore

after the organic groups' removal by calcination: the Brønsted acid sites can be formed in both calcined samples in situ upon the action of water originating in ethanol dehydration (although the initially hybrid sample **p_PhCH$_2$-500** still exhibited a much lower B/L ratio).

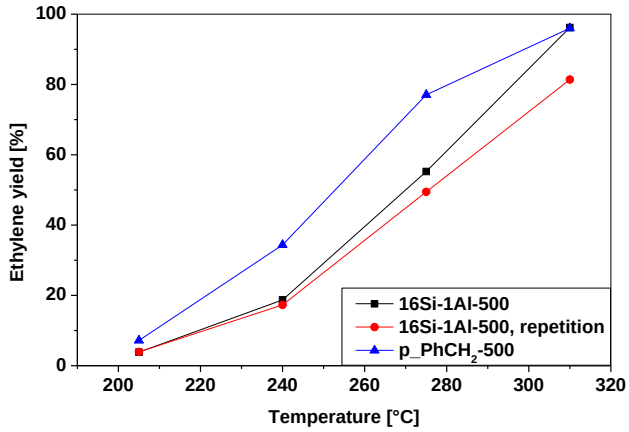

Fig. 9: Ethylene yield in gas phase ethanol dehydration over aluminosilicate catalysts calcined at 500 °C.

Three commercial reference catalysts were tested at identical conditions for comparison and reported earlier: silica-alumina catalysts support (grade 135), γ-alumina, and HZSM-5 [12, 49]. All NHSG-prepared aluminosilicate catalysts (both hybrid and fully inorganic) exhibited ethanol conversion in between poorly active commercial silica-alumina and γ-alumina and highly active HZSM-5, similar to previous reports on NHSG-prepared aluminosilicate catalysts (Table 2S). Ethylene selectivity shown by NHSG-prepared catalysts was high (outperforming HZSM-5 at 205 °C; Table 2S), pointing at the crucial role of strong Lewis acid sites in NHSG-prepared materials [12, 49] either in a direct ethanol dehydration to ethylene or an indirect path via diethylether decomposition to ethylene and water [67, 71, 72].

Conclusions

In summary, we have prepared hybrid aluminosilicates containing various organic groups (pendant benzyl and methyl; bridging methylene, ethylene, and xylylene) prepared by one-

pot non-hydrolytic sol-gel. The Si:Al ratio was 16 in all samples; one Si atom out of 16 was bound to an organic group (samples contained 15 SiO_4 units per one $RSiO_3$ group in case of terminal organic groups and 30 SiO_4 units per one $O_3Si–R–SiO_3$ moiety). The presence of organic groups was confirmed by MAS NMR, IR, XPS, and ToF-SIMS analyses. The addition of organic groups did not markedly alter the structure (IR, MAS NMR), the porosity (N_2 adsorption-desorption experiments), or the hydrophilicity (water adsorption and contact angle) of aluminosilicate catalysts. On the contrary, the addition of organic groups induced slight changes in the homogeneity of Si-Al mixing, which was studied by ToF-SIMS analyses in the outermost surface layer: the presence of aromatic organic groups seemed to be beneficial and increased the dispersion of Al forming more isolated species. This in turn led to variations in the numbers of acid sites: aluminosilicate catalysts containing benzyl and xylylene organic groups exhibited higher acid site numbers, while catalysts with methylene and ethylene bridges showed lower acid site numbers. This appears to be directly associated with the catalyst activity, as the conversion is dictated by the number of acid sites. Finally, the presence of organic groups also influenced Brønsted-to-Lewis ratios: all hybrid catalysts displayed lower B/L ratio than pure inorganic **16Si-1Al**, probably due to a lower Si–OH groups content (these were substituted by Si-R groups). This is associated with a higher selectivity for ethylene at the expense of diethyl ether.

Acknowledgments

A.S. acknowledges funding from the European Union´s Horizon 2020 research and innovation programme under the Marie Skłodowska-Curie grant agreement No 751774. F.R.S.–F.N.R.S. is thanked for the acquisition of the physi-chemisorption equipment (project "EQP U.N030.18"). Authors acknowledge the 'Communauté française de Belgique' for the financial support through the ARC programme (15/20-069). This research used resources of the "Plateforme Technologique Physico-Chemical Characterization" – PC^2, the SIAM platform (Synthesis, Irradiation & Analysis of Materials) and the MORPH-IM platform (Morphology & Imaging) located at the University of Namur. The work has been financially supported by the Czech Science Foundation under the project GJ20-03636Y. D.P. Debecker thanks the Francqui Foundation for his "Francqui Research Professor" chair. J.F. Statsyns is acknowledged for the technical help.

Conflict of interest

The authors declare no conflict of interest.

References

1. Faustini M, Nicole L, Ruiz-Hitzky E, Sanchez C (2018) History of Organic-Inorganic Hybrid Materials: Prehistory, Art, Science, and Advanced Applications. Adv Funct Mater 28:1704158. https://doi.org/10.1002/adfm.201704158

2. De Clippel F, Dusselier M, Van De Vyver S, et al (2013) Tailoring nanohybrids and nanocomposites for catalytic applications. Green Chem 15:1398–1430. https://doi.org/10.1039/c3gc37141g

3. Bispo C, Ferreira P, Trouvé A, et al (2013) Role of acidity and hydrophobicity in the remarkable catalytic activity in water of sulfonic acid-functionalized phenyl-PMO materials. Catal Today 218–219:85–92. https://doi.org/10.1016/j.cattod.2013.06.004

4. An S, Sun Y, Song D, et al (2016) Arenesulfonic acid-functionalized alkyl-bridged organosilica hollow nanospheres for selective esterification of glycerol with lauric acid to glycerol mono- and dilaurate. J Catal 342:40–54. https://doi.org/10.1016/j.jcat.2016.07.004

5. Sánchez-Vázquez R, Pirez C, Iglesias J, et al (2013) Zr-Containing Hybrid Organic-Inorganic Mesoporous Materials: Hydrophobic Acid Catalysts for Biodiesel Production. ChemCatChem 5:994–1001. https://doi.org/10.1002/cctc.201200527

6. Smeets V, Ben Mustapha L, Schnee J, et al (2018) Mesoporous SiO2-TiO2 epoxidation catalysts: Tuning surface polarity to improve performance in the presence of water. Mol Catal 452:123–128. https://doi.org/10.1016/j.mcat.2018.04.011

7. Lorret O, Lafond V, Mutin PH, Vioux A (2006) One-Step Synthesis of Mesoporous Hybrid Titania−Silica Xerogels for the Epoxidation of Alkenes. Chem Mater 18:4707–

4709. https://doi.org/10.1021/cm061478q

8. Melero JA, van Grieken R, Morales G (2006) Advances in the synthesis and catalytic applications of organosulfonic-functionalized mesostructured materials. Chem Rev 106:3790–3812. https://doi.org/10.1021/cr050994h

9. Gounder R, Davis ME (2013) Monosaccharide and disaccharide isomerization over Lewis acid sites in hydrophobic and hydrophilic molecular sieves. J Catal 308:176–188. https://doi.org/10.1016/j.jcat.2013.06.016

10. Vivian A, Fusaro L, Debecker DP, Aprile C (2018) Mesoporous Methyl-Functionalized Sn-Silicates Generated by the Aerosol Process for the Sustainable Production of Ethyl Lactate. ACS Sustain Chem Eng 6:14095–14103. https://doi.org/10.1021/acssuschemeng.8b02623

11. Silvestre-Alberó J, Domine ME, Jordá JL, et al (2015) Spectroscopic, calorimetric, and catalytic evidences of hydrophobicity on Ti-MCM-41 silylated materials for olefin epoxidations. Appl Catal A Gen 507:14–25. https://doi.org/10.1016/j.apcata.2015.09.029

12. Styskalik A, Kordoghli I, Poleunis C, et al (2020) Hybrid mesoporous aluminosilicate catalysts obtained by non-hydrolytic sol-gel for ethanol dehydration. J Mater Chem A 8:23526–23542. https://doi.org/10.1039/d0ta07016e

13. Vivian A, Soumoy L, Fusaro L, et al (2020) Surface-functionalized mesoporous gallosilicate catalysts for the efficient and sustainable upgrading of glycerol to solketal. Green Chem. https://doi.org/10.1039/d0gc02562c

14. Vriamont C, Devillers M, Riant O, Hermans S (2013) Catalysis with Gold Complexes

Immobilised on Carbon Nanotubes by π-π Stacking Interactions: Heterogeneous Catalysis versus the Boomerang Effect. Chem - A Eur J 19:12009–12017. https://doi.org/10.1002/chem.201300998

15. Styskalik A, Skoda D, Moravec Z, et al (2015) Control of micro/mesoporosity in non-hydrolytic hybrid silicophosphate xerogels. J Mater Chem A 3:7477–7487. https://doi.org/10.1039/C4TA06823H

16. Machac P, Alauzun JG, Styskalik A, et al (2021) Synthesis of high surface area aluminophosphate and -phosphonate xerogels by non-hydrolytic sol-gel reactions. Microporous Mesoporous Mater 311:. https://doi.org/10.1016/j.micromeso.2020.110682

17. Shylesh S, Samuel PP, Singh AP (2007) Synthesis of hydrothermally stable aluminium-containing ethane-silica hybrid mesoporous materials using different aluminium sources. Microporous Mesoporous Mater 100:250–258. https://doi.org/10.1016/J.MICROMESO.2006.11.010

18. Styskalik A, Abbott JG, Orick MC, et al (2018) Synthesis , characterization and catalytic activity of single site , Lewis acidic aluminosilicates. Catal Today 1–9. https://doi.org/10.1016/j.cattod.2018.11.079

19. Dacquin JP, Cross HE, Brown DR, et al (2010) Interdependent lateral interactions, hydrophobicity and acid strength and their influence on the catalytic activity of nanoporous sulfonic acid silicas. Green Chem 12:1383–1391. https://doi.org/10.1039/c0gc00045k

20. Wang Y, Alauzun JG, Mutin PH (2020) Water-Stable, Nonsiliceous Hybrid Materials with Tunable Porosity and Functionality: Bridged Titania-Bisphosphonates. Chem

Mater 32:2910–2918. https://doi.org/10.1021/acs.chemmater.9b05095

21. Livage J (1998) Sol-gel synthesis of heterogeneous catalysts from aqueous solutions. Catal Today 41:3–19. https://doi.org/10.1016/S0920-5861(98)00034-0

22. Debecker DP (2018) Innovative Sol-Gel Routes for the Bottom-Up Preparation of Heterogeneous Catalysts. Chem Rec 18:662–675. https://doi.org/10.1002/tcr.201700068

23. Debecker DP, Mutin PH (2012) Non-hydrolytic sol-gel routes to heterogeneous catalysts. Chem Soc Rev 41:3624–3650. https://doi.org/10.1039/C2CS15330K

24. Styskalik A, Skoda D, Barnes CE, Pinkas J (2017) The Power of Non-Hydrolytic Sol-Gel Chemistry: A Review. Catalysts 7:168. https://doi.org/10.3390/catal7060168

25. Smeets V, Styskalik A, Debecker DP (2021) Non-hydrolytic sol–gel as a versatile route for the preparation of hybrid heterogeneous catalysts. J Sol-Gel Sci Technol 1–18. https://doi.org/10.1007/s10971-021-05486-1

26. Skoda D, Styskalik A, Moravec Z, et al (2016) Novel non-hydrolytic templated sol–gel synthesis of mesoporous aluminosilicates and their use as aminolysis catalysts. RSC Adv 6:24273–24284. https://doi.org/10.1039/C5RA24563J

27. Styskalik A, Skoda D, Moravec Z, et al (2016) Surface reactivity of non-hydrolytic silicophosphate xerogels: a simple method to create Brønsted or Lewis acid sites on porous supports. New J Chem 40:3705–3715. https://doi.org/10.1039/C5NJ02928G

28. Styskalik A, Kordoghli I, Poleunis C, et al (2020) Highly porous hybrid metallosilicate materials prepared by non-hydrolytic sol-gel: Hydrothermal stability and catalytic properties in ethanol dehydration. Microporous Mesoporous Mater 297:110028.

https://doi.org/10.1016/j.micromeso.2020.110028

29. de Lima OJ, de Aguirre DP, de Oliveira DC, et al (2001) Porphyrins entrapped in an alumina matrix. J Mater Chem 11:2476–2481. https://doi.org/10.1039/b100897h

30. Zhang R, Russo PA, Buzanich AG, et al (2017) Hybrid Organic–Inorganic Transition-Metal Phosphonates as Precursors for Water Oxidation Electrocatalysts. Adv Funct Mater 27:1–11. https://doi.org/10.1002/adfm.201703158

31. Capeletti LB, do Carmo Martins Alves M, Cardoso MB, dos Santos JHZ (2018) Hybrid silica based catalysts prepared by the encapsulation of zirconocene compound via non-hydrolytic sol-gel method for ethylene polymerization. Appl Catal A Gen 560:225–235. https://doi.org/10.1016/j.apcata.2018.03.013

32. Ullmann MA, dos Santos JHZ (2020) Zirconocene immobilization into organic-inorganic dual-shell silicas prepared by the nonhydrolytic sol-gel method for polyethylene production. J Catal 385:30–43. https://doi.org/10.1016/j.jcat.2020.03.001

33. Ullmann MA, dos Santos JHZ (2019) Deactivation study of zirconocene immobilization into Lewis acid and dual-shell silicas prepared by a nonhydrolytic sol-gel method. J Catal 378:226–237. https://doi.org/10.1016/j.jcat.2019.08.040

34. Fisch AG, Cardozo NSM, Secchi AR, et al (2008) Investigation of silica particle structure containing metallocene immobilized by a sol–gel method. J Non Cryst Solids 354:3973–3979. https://doi.org/10.1016/j.jnoncrysol.2008.05.018

35. Fisch AG, Da Silveira N, Cardozo NSM, et al (2013) Direct production of ultra-high molecular weight polyethylene with oriented crystalline microstructures. J Mol Catal A Chem 366:74–83. https://doi.org/10.1016/j.molcata.2012.08.028

36. Caiut JMA, Nakagaki S, De Lima OJ, et al (2003) Encapsulation of Tetraazaannulenato Compounds in Matrix by Sol-Gel Process. J Sol-Gel Sci Technol 28:57–64. https://doi.org/10.1023/A:1025685019670

37. Mac Leod TCO, Guedes DFC, Lelo MR, et al (2006) Catalytic activity of Jacobsen catalyst encapsulated in an alumina matrix by the sol-gel process. J Mol Catal A Chem 259:319–327. https://doi.org/10.1016/j.molcata.2006.07.022

38. Saltarelli M, de Faria EH, Ciuffi KJ, et al (2019) Aminoiron(III)–porphyrin–alumina catalyst obtained by non-hydrolytic sol-gel process for heterogeneous oxidation of hydrocarbons. Mol Catal 462:114–125. https://doi.org/10.1016/j.mcat.2018.09.014

39. Behrens M, Datye AK (2013) Catalysis for the Conversion of Biomass and Its Derivatives. Ed. Open Access, Berlin

40. Angelici C, Weckhuysen BM, Bruijnincx PCA (2013) Chemocatalytic conversion of ethanol into butadiene and other bulk chemicals. ChemSusChem 6:1595–1614. https://doi.org/10.1002/cssc.201300214

41. Sun J, Wang Y (2014) Recent advances in catalytic conversion of ethanol to chemicals. ACS Catal 4:1078–1090. https://doi.org/10.1021/cs4011343

42. Debecker DP, Boissière C, Laurent G, et al (2015) First acidic macro-mesocellular aluminosilicate monolithic foams “SiAl(HIPE)” and their catalytic properties. Chem Commun 51:14018–14021. https://doi.org/10.1039/C5CC05328E

43. Zhang M, Yu Y (2013) Dehydration of ethanol to ethylene. Ind Eng Chem Res 52:9505–9514. https://doi.org/10.1021/ie401157c

44. Fan D, Dai DJ, Wu HS (2013) Ethylene formation by catalytic dehydration of ethanol

with industrial considerations. Materials (Basel) 6:101–115. https://doi.org/10.3390/ma6010101

45. Shen JGC, Herman RG, Klier K (2002) Sulfonic acid-functionalized mesoporous silica: Synthesis, characterization, and catalytic reaction of alcohol coupling to ethers. J Phys Chem B 106:9975–9978. https://doi.org/10.1021/jp020131h

46. van Grieken R, Melero JA, Morales G (2006) Etherification of benzyl alcohols with 1-hexanol over organosulfonic acid mesostructured materials. J Mol Catal A Chem 256:29–36. https://doi.org/10.1016/j.molcata.2006.04.040

47. Sow B, Hamoudi S, Hassan Zahedi-Niaki M, Kaliaguine S (2005) 1-Butanol Etherification Over Sulfonated Mesostructured Silica and Organo-Silica. Microporous Mesoporous Mater 79:129–136. https://doi.org/10.1016/j.micromeso.2004.10.038

48. Liu J, Yang J, Li C, Yang Q (2009) Catalytic applications of sulfonic acid functionalized mesoporous organosilicas with different fraction of organic groups in the pore wall. J Porous Mater 16:273–281. https://doi.org/10.1007/s10934-008-9197-8

49. Styskalik A, Vykoukal V, Fusaro L, et al (2020) Mildly acidic aluminosilicate catalysts for stable performance in ethanol dehydration. Appl Catal B Environ 118926. https://doi.org/10.1016/j.apcatb.2020.118926

50. Motevalli M, Ou DL, Sullivan AC (1993) Synthesis and characterization of bis(trichlorosilylmethyl)benzenes. J Organomet Chem 445:35–38. https://doi.org/10.1016/0022-328X(93)80183-C

51. Emeis C. A. (1993) Determination of integrated molar extinction coefficients for Infrared absorption Bands of Pyridine Adsorbed on Solid Acid Catalysts. J. Catal.

141:347–354

52. Rouquerol J, Rouquerol F, Sing KSW (1998) Adsorption by Powders and Porous Solids. Academic Press

53. Lowell S (2004) Characterization of Porous Solids and Powders: Surface Area, Pore Size and Density. Springer

54. Olson DH, Haag WO, Borghard WS (2000) Use of water as a probe of zeolitic properties: Interaction of water with HZSM-5. Microporous Mesoporous Mater 35–36:435–446. https://doi.org/10.1016/S1387-1811(99)00240-1

55. Thommes M, Mitchell S, Pérez-Ramírez J (2012) Surface and pore structure assessment of hierarchical MFI zeolites by advanced water and argon sorption studies. J Phys Chem C 116:18816–18823. https://doi.org/10.1021/jp3051214

56. Shirley DA (1972) High-Resolution X-Ray Photoemission Spectrum of the Valence Bands of Gold. Phys Rev B 5:4709–4714. https://doi.org/10.1103/PhysRevB.5.4709

57. Debecker DP, Hulea V, Mutin PH (2013) Mesoporous mixed oxide catalysts via non-hydrolytic sol–gel: A review. Appl Catal A Gen 451:192–206. https://doi.org/10.1016/j.apcata.2012.11.002

58. Crouzet L, Leclercq D, Mutin PH, Vioux A (2003) Organic-inorganic materials by nonhydrolytic sol-gel processes: Organosilsesquioxane-metal oxide hybrids. J Sol-Gel Sci Technol 26:335–338. https://doi.org/10.1023/A:1020792208751

59. Kriesel JW, Sander MS, Tilley TD (2001) Block Copolymer-Assisted Synthesis of Mesoporous, Multicomponent Oxides by Nonhydrolytic, Thermolytic Decomposition of Molecular Precursors in Nonpolar Media. Chem Mater 13:3554–3563.

https://doi.org/10.1021/cm010068t

60. Hirata Y, Sakeda K, Matsushita Y, et al (1989) Characterization and Sintering Behavior of Alkoxide-Derived Aluminosilicate Powders. J Am Ceram Soc 72:995–1002. https://doi.org/10.1111/j.1151-2916.1989.tb06258.x

61. Ruiz de Sola E, Estevan F, Torres FJ, Alarcón J (2005) Effect of thermal treatment on the structural evolution of 3:2 and 2:1 mullite monophasic gels. J Non Cryst Solids 351:1202–1209. https://doi.org/10.1016/j.jnoncrysol.2005.02.017

62. Blackwell CS (1979) Investigation of zeolite frameworks by vibrational properties. 1. The double-four-ring in group 3 zeolites. J Phys Chem 83:3251–3257. https://doi.org/10.1021/j100488a014

63. Handke M, Kowalewska A (2011) Siloxane and silsesquioxane molecules - Precursors for silicate materials. In: Spectrochimica Acta - Part A: Molecular and Biomolecular Spectroscopy. Elsevier, pp 749–757

64. Hong SH, Hyun S Il, Jung IN, et al (2010) [Bu4P]+Cl--catalyzed reactions of trichlorosilane and dichloromethylsilane with vinyltrichlorosilane: New synthetic method for 1,1,4,4-tetrachloro-2,5-bis(trichlorosilyl)-1, 4-disilacyclohexane compounds. Organometallics 29:3054–3057. https://doi.org/10.1021/om100039b

65. Hong SH, Hyun S Il, Jung IN, et al (2010) Phosphine-Catalyzed Si-C Coupling of Bissilylmethanes: Preparation of Cyclic (Cl2SiCH2)2 and Linear Cl 2Si(CH2SiCl3)2 via Silylene and Silene Intermediates. Organometallics 29:687–691. https://doi.org/10.1021/om901071k

66. Van Bokhoven JA, Van der Eerden AMJ, Koningsberger DC (2003) Three-coordinate

aluminum in zeolites observed with in situ x-ray absorption near-edge spectroscopy at the Al K-edge: Flexibility of aluminum coordinations in zeolites. J Am Chem Soc 125:7435–7442. https://doi.org/10.1021/ja0292905

67. Wang Z, O'Dell LA, Zeng X, et al (2019) Insight into Three-Coordinate Aluminum Species on Ethanol-to-Olefin Conversion over ZSM-5 Zeolites. Angew Chemie Int Ed 58:18061–18068. https://doi.org/10.1002/anie.201910987

68. Hensen EJM, Poduval DG, Degirmenci V, et al (2012) Acidity characterization of amorphous silica-alumina. J Phys Chem C 116:21416–21429. https://doi.org/10.1021/jp309182f

69. Leydier F, Chizallet C, Chaumonnot A, et al (2011) Brønsted acidity of amorphous silica-alumina: The molecular rules of proton transfer. J Catal 284:215–229. https://doi.org/10.1016/j.jcat.2011.08.015

70. Chizallet C (2020) Towards the Atomic Scale Simulation of Intricate Acidic Aluminosilicate Catalysts. ACS Catal. https://doi.org/10.1021/acscatal.0c01136

71. Phung TK, Proietti Hernández L, Lagazzo A, Busca G (2015) Dehydration of ethanol over zeolites, silica alumina and alumina: Lewis acidity, Brønsted acidity and confinement effects. Appl Catal A Gen 493:77–89. https://doi.org/10.1016/j.apcata.2014.12.047

72. Phung TK, Busca G (2015) Ethanol dehydration on silica-aluminas: Active sites and ethylene/diethyl ether selectivities. Catal Commun 68:110–115. https://doi.org/10.1016/J.CATCOM.2015.05.009